Journal of Saudi Chemical Society (2020) **24**, 811–823

King Saud University

Journal of Saudi Chemical Society

www.ksu.edu.sa
www.sciencedirect.com

ORIGINAL ARTICLE

Characterization and Artificial Neural Networks Modelling of methylene blue adsorption of biochar derived from agricultural residues: Effect of biomass type, pyrolysis temperature, particle size

Ammar Albalasmeh [a,*,1], Mamoun A. Gharaibeh [a], Osama Mohawesh [b], Mohammad Alajlouni [a], Mohammed Quzaih [a], Mohanad Masad [c], Ali El Hanandeh [d,*,1]

[a] *Department of Natural Resources and Environment, Faculty of Agriculture, Jordan University of Science and Technology, Irbid 22110, Jordan*
[b] *Department of Plant Production, Faculty of Agriculture, Mutah University, Karak, Jordan*
[c] *Water Environment and Arid Region Research Center, Al al-Bayt University, Al-Mafraq 25113, Jordan*
[d] *School of Engineering and Built Environment, Griffith University Nathan, Australia*

Received 30 April 2020; revised 25 June 2020; accepted 5 July 2020
Available online 12 July 2020

KEYWORDS

Biochar;
Slow pyrolysis;
Characterization;
Agricultural wastes;
Pyrolysis temperature;
Artificial Neural Networks

Abstract Biochar has been explored as a sorbent for contaminants, soil amendment and climate change mitigation tool through carbon sequestration. Through the optimization of the pyrolysis process, biochar can be designed with qualities to suit the intended uses. Biochar samples were prepared from four particle sizes (100–2000 μm) of three different feedstocks (oak acorn shells, jift and deseeded carob pods) at different pyrolysis temperatures (300–600 °C). The effect of these combinations on the properties of the produced biochar was studied. Biochar yield decreased with increasing pyrolysis temperature for all particle sizes of the three feedstocks. Ash content, fixed carbon, thermal stability, pH, electrical conductivity (EC), specific surface area (SSA) of biochar increased

* Corresponding authors at: Environmental Soil Physics, Department of Natural Resources and Environment Faculty of Agriculture, Jordan University of Science and Technology, Jordan (A. Albalasmeh). School of Engineering and Built Environment, Griffith University, Nathan, QLD 4111, Australia (A. El Hanandeh).
E-mail addresses: aalbalasmeh@just.edu.jo (A. Albalasmeh), a.elhanandeh@griffith.edu.au (A. El Hanandeh), a.elhanandeh@griffith.edu.au (A. El Hanandeh).
[1] Contributed equally.

Peer review under responsibility of King Saud University.

Production and hosting by Elsevier

https://doi.org/10.1016/j.jscs.2020.07.005

with increasing pyrolysis temperature. Volatile matter and pH value at the point of zero charge (pH_{pzc}) of biochar decreased with increasing pyrolysis temperature. Fourier-transform infrared spectroscopy (FTIR) analysis indicated that the surface of the biochar was rich with hydroxyl, phenolic, carbonyl and aliphatic groups. Methylene blue (MB) adsorption capacity was used as an indicator of the quality of the biochar. Artificial neural networks (ANN) model was developed to predict the quality of the biochar based on operational conditions of biochar production (parent biomass type, particle size, pyrolysis temperature). The model successfully predicted the MB adsorption capacity of the biochar. The model is a very useful tool to predict the performance of biochar for water treatment purposes or assessing the general quality of a design biochar for specific application.

1. Introduction

The continuous increase in world population and therefore the demand for food and energy has led to more by-products and an increase in the amount of agricultural residues [1]. Meanwhile there is a rising interest in the concept of zero waste and circular economy [2]. The production of biochar from agricultural waste can contribute towards achieving the concept of "zero waste" and circular economy concepts by converting the agricultural waste into beneficial and sustainable by-products and in contrast with current waste management practice of landfilling or burning; a significant source of air pollution [3–6].

Biochar is defined as a porous, low density, and carbon rich material obtained from thermochemical conversion of biomass under controlled conditions (oxygen-limited environment and low temperature) [7,8]. Over the last decade, biochar produced from different biomasses has been studied extensively in various energy and environmental applications including soil and water remediation [4,8–12]. For instance, when biochar is applied to soil it improves physical and chemical properties of the soil (soil structure, cation exchange capacity, soil water and nutrient retention, soil bulk density, etc.) and consequently increases crop productivity [13–16]. Moreover, biochar can be used as a tool to reduce global warming through carbon sequestration due to its resistance to chemical and biological decomposition [6].

Because of the widespread use of feedstocks which can be used for biochar production and the variation in the physical and chemical properties of the original biomass, it is important to examine the effect of pyrolysis conditions on biochar properties [2]. For example, Ahmed et al. [17] produced biochar from 32 different feedstocks that differ in their properties [17]. Biochar properties are not only influenced by the type of feedstock (biomass type, particle size, etc.), but also by pyrolysis conditions (temperature, heating rate, vapor retention time, etc.) [2,4]. Understanding the effect of these combinations on the resulting biochar is necessary for adequate decision towards proceeding in biochar production [3,18,19]. Therefore, several researchers investigated the relationship between different feedstocks and pyrolysis conditions.

From the pyrolysis conditions, charring temperature plays a significant role in the properties of the produced biochar [15]. For instance, specific surface area increased significantly as charring temperature increased from 350 to 450 to 550 °C [2] which reflects positively on contaminant adsorption capacity [20]. Also, it affects the pH which influences the heavy metals mobilization in the treated soil [21,22]. Moreover, biochars produced at higher pyrolysis temperature reduce the capacity for nutrient retention in the treated soil [1]. Meanwhile, it becomes resistant to decomposition in soil, which makes it a good option for carbon sequestration [15,23,24]. In contrast, the biochar produced at lower pyrolysis temperature has higher volatile matter, higher yield and lower pH compared to that produced at higher pyrolysis temperature [15,25].

The other important parameter of biochar production is feedstock's characteristics; therefore biochar produced under the same pyrolysis conditions will have different properties [15]. For example, the amount of nutrients will depend on the feedstock type, i.e. biochar produced from manure is considered as source of phosphorus (P) [26] and nitrogen (N) [27]. At the same time, it promotes soil microbial abundance more than the other biochar derived from other feedstocks [28]. Moreover, wood based biochar demonstrated a better adsorption capacity compared to biochar produced from rice materials [29].

Due to the above-mentioned differences and the different applications of biochar and to satisfy stakeholders requirements, the physical and chemical properties of the biochar produced from different feedstocks under different pyrolysis conditions need to be characterized and fully understood.

Methylene blue (MB) adsorption capacity is a good indicator of carbonaceous materials activity [30]. It is also an excellent indicator of the mesoporous surface area of the biochar (2–50 nm). Mesoporosity is an important characteristic of carbon materials especially for the adsorption of large molecules such as dyes [31]. Furthermore, as it is a cationic dye it is also a good indicator of the biochar's capacity for the removal of heavy metals cations [32]. As such, many researchers have used MB adsorption capacities as a convenient, low cost-cost and low-hazard indicator of the biochar's performance.

As biochar can be used for different applications, it is important to be able to predict the performance of the material before committing to its pre-recruitment or production. Computer modelling and simulations are effective methods to do so. Artificial neural networks (ANN) are among the most promising methods.

Several researchers applied ANN to model the adsorption process of different sorbates onto different adsorbents. Ghaedi and Vafaei [33] reviewed the application of ANN to the adsorption of dyes. Karimi and Ghaedi [34] applied ANN and Genetic algorithm techniques to model the adsorption of

MB onto activated carbon (AC). Their model focuses on the optimization of the adsorption process (pH, contact time, mixing rate, initial concentration of MB and the dose rate of AC). Mahmoodi-Babolan et al. [35] used ANN-particle swarm optimization to model the adsorption of MB on super sorbent derived from potato starch and catecholamine and compared the performance of the ANN response surface methodology (RSM). In their model they focused on the adsorption process optimization factors (contact time, initial concentration of MB and pH). And most recently, Jun et al. [36] used a similar approach to model the adsorption of MB by Buckypaper/Polyvinyl alcohol treated with jicama peroxidase (JP). In addition to the pH, MB concentration and contact time, they considered the effect of JP concentration on the adsorption capacity. Despite the good modelling results obtained in the previous studies, the models were designed using specific adsorbent and did not consider the adsorbent characteristics. Souza et al. [37] developed an ANN model to predict the Ni^{2+} adsorption capacity of biochars prepared from different biomass. However, in their model they used the surface area of the biochar, the adsorbate dose, the point of zero charge (pH_{pzc}) and contact time as the predictors, thus ignoring the origin of the biochar and production conditions. Although this is a useful approach to select a biochar from a set to optimize the adsorption, it cannot be used to determine the operational conditions to design a biochar. Another limitation of the reviewed works was the use of a small data set (< 70). This can be an issue as ANN are data driven and their training requires a significant amount of data to prevent the network from memorizing the training set. Therefore, the objectives of this study were to (1) assess the physicochemical properties of the produced biochar as a function of feedstock type, size and pyrolysis temperature; (2) assess their adsorption capacity for MB as an indicator of their activity and finally (3) develop an ANN model to predict the adsorption capacity of the biochar for MB. Up to our knowledge, this is the first study that has incorporated the biomass type, particle size and the pyrolysis temperature effects on the resultant biochar adsorption capacity into ANN model.

2. Materials and methods

2.1. Feedstocks collection and preparation

Three different waste biomass materials (feedstocks) were used to produce biochar in this study: (i) solid olive mill waste, locally known as Jift, collected from Al-Yarmouk olive mill, Irbid Jordan (ii) oak acorn shells (oak) collected from Jerash forests, Jordan and (iii) deseeded carob pods (carob) collected from Jordan university of science and technology campus, Jordan. The raw materials were first air-dried and then placed in an oven at 50 °C until constant weight was achieved. After that, all feedstocks were ground and sieved to the following classes: 100–300 μm, 300–500 μm, 500–1000 μm and 1000–2000 μm.

2.2. Biochar preparation

Measured quantities of the feedstocks were placed in crucibles and were tightly covered with aluminum foil to limit oxygen supply. The crucibles were heated in an electrical muffle furnace (N60/H, Hermes Electronic, Germany) from room temperature to the desired temperature (300, 400, 500, and 600 °C). The target temperature was maintained for 1.5 h then the furnace was allowed to cool down to room temperature before samples were retrieved. Finally, biochar samples were stored in airtight containers for further analysis. All experiments were conducted in triplicates. The produced biochars were labeled according to their pyrolysis temperature and parent biomass particle size as illustrated in Table 1.

2.3. Biochar characterization

2.3.1. Biochar yield, electrical conductivity, pH and pH_{pzc}

Biochar yield was measured as the ratio of mass of biochar produced after pyrolysis relative to the original mass of feedstock. The electrical conductivity (EC) was measured using 1:20 solution of biochar in water [38]. The mixture was stirred for 20 min. and EC was measured using Orion EC meter (Thermo scientific, Orion Star A212 Conductivity Benchtop meter). The pH value of biochar was measured according to the ASTM D3838-05. Boiling water was added to biochar at the ratio of 1:10. After stirring and filtration then cooling the filtrate to room temperature, pH was measured using Orion pH meter (Thermo scientific, Orion Star A211 pH Benchtop meter).

The pH value at the point of zero charge of biochar (pH_{pzc}) was measured using mass titration method [39]. In brief, a series of biochar mass was mixed with a 25 mL of 0.03 M KNO_3. The pH_{pzc} is the pH at which a plateau is achieved when plotting biochar mass versus equilibrium pH.

2.3.2. Proximate analysis

Ash content (ASH) of biochar samples was determined according to the ASTM Standard Method (D 3174) by a sample mass difference after combusting 1 g of biochar placed in an open crucible in a muffle furnace (N60/H, Hermes Electronic, Germany) at 750 °C for 6 h. Similarly, volatile matter content (VM) was determined according to ASTM Standard Method (D 1762-84) by a sample mass difference after combusting 1 g of biochar sample placed in a closed crucible in a muffle furnace (N60/H, Hermes Electronic, Germany) at 950 °C for 11 min. to measure mass loss due to volatilization of volatile components. Fixed carbon content (FC) was calculated as the difference between 100 and the sum of ASH and VM contents. Lastly, biochar thermal stability (TS) was calculated as the ratio between fixed carbon and the sum of FC and VM. Values closer to one indicate more stable biochar [40].

2.3.3. Methylene blue adsorption and surface area estimation

The specific surface area of biochar (SSA) was measured using the methylene blue (MB) method [41]. A stock solution of 2 g L^{-1} MB was prepared and allowed to stand overnight. The stock was then used to prepare working dilutions of 1, 2, 3, 4 and 5 mM. Then, 1 g of biochar (crushed to pass through 0.6 mm sieve) was mixed with 50 mL of MB solution at different concentrations (1, 2, 3, and 5 mM) under room temperature condition. After 48 h of settling time to reach equilibrium, sample was withdrawn and the residual concentration of MB was measured using UV–VIS spectrophotometer (photoLab 7600 UV–VIS, WTW GmbH, Germany) at

Table 1 Coded level of treatments used in biochar characterization.

Feedstock	Size (μm)	Temperature (°C)			
		300	400	500	600
Jift	100–300	J300-100	J400-100	J500-100	J600-100
	300–500	J300-300	J400-300	J500-300	J600-300
	500–1000	J300-500	J400-500	J500-500	J600-500
	1000–2000	J300-1000	J400-1000	J500-1000	J600-1000
Oak acorns	100–300	O300-100	O400-100	O500-100	O600-100
	300–500	O300-300	O400-300	O500-300	O600-300
	500–1000	O300-500	O400-500	O500-500	O600-500
	1000–2000	O300-1000	O400-1000	O500-1000	O600-1000
Carob pods	100–300	C300-100	C400-100	C500-100	C600-100
	300–500	C300-300	C400-300	C500-300	C600-300
	500–1000	C300-500	C400-500	C500-500	C600-500
	1000–2000	C300-1000	C400-1000	C500-1000	C600-1000

wavelength of 664 nm. The amount of methylene blue adsorbed on the biochar (q_e) is calculated as

$$q_e = \frac{(C_i - C_e) \times V}{M}$$

where C_i (mg L^{-1}) is the initial concentration of MB solution at starting time (t = 0), C_e (mg L^{-1}) is the concentration of MB solution at equilibrium time, V (L) is the volume of the solution treated and M (g) is the mass of the biochar. Each experiment was repeated 3 times.

Finally, specific surface area of biochar was calculated according to the following equation:

$$SSA = \frac{q_{MB} \times N_A \times A_{MB}}{1000}$$

where SSA is the specific surface area, q_{MB} is the amount of methylene blue adsorbed on the biochar (mmol g^{-1}) obtained from the mono-layer adsorption isotherm using Langmuir equation, N_A is the avogadro's number (6.023×10^{23} mol^{-1}) and A_{MB} is the area covered by one MB molecule (130 $Å^2$). The Langmuir isotherm equation is presented as follows:

$$q_e = \frac{q_{MB} \times K_L \times C_e}{(1 + K_L \times C_e)}$$

where q_e is the adsorption capacity (mmol.g^{-1}), q_{MB} is the maximum adsorption capacity (mmol.g^{-1}), K_L is Langmuir constant (L.g^{-1}), Ce is concentration at equilibrium (mmol. L^{-1}).

2.3.4. Fourier-transform infrared spectroscopy (FTIR)

The biochar was analyzed using FTIR analysis to determine the surface functional groups. FTIR analysis was carried out by mixing a small amount of the sample with KBr and then the sample was scanned using IRAffinity-1S spectrophotometer (Shimadzu, Japan) over a range of 400–4000 cm^{-1} with a resolution factor of 4 cm^{-1}.

2.3.5. Artificial Neural Network modelling

Artificial Neural Network models are a group of data-driven models that are used for prediction of output based on discovering and mapping relations using a set of input independent variables to target values. Feed forward back propagation ANN is a classic architecture used for predictive models. The general architecture of the model is composed of an input layer, a hidden layer and an output layer. The hidden layer can have a number of neurons which are governed by an activation function. The activation function is dependent on a weighting (w) and a bias (b). The following Fig. 1 represents a network with 3 input variables, 1 hidden layer with 2 neurons and an output layer with 2 neurons. In a general form, the system can be represented as [42]:

$$Y_j^{k+1} = f(\sum_{i=1}^{N} X_i^k w_{ij}^k + b_i^k)$$

where f is the activation function, N number of inputs of the neuron and k is the layer (hidden, output).

3. Results and discussion

3.1. Biochar yield

Fig. 2 shows the effect of pyrolysis temperatures and feedstock types and sizes on biochar yield. All results show a non-linear decrease for biochar yield with an increase in the pyrolysis temperature (R^2 = 0.76) for all feedstocks and different sizes (Fig. 2a). The maximum and minimum yield of Oak acorn-biochar was 67% and 27% for O300-300 and O600-500, respectively (Fig. 2b). Whereas the maximum yield for the biochar produced from Jift was 55% for J300-300 and the minimum yield was 28% (Fig. 2c). Similarly, the maximum yield for the biochar produced from Carob pods was equal for C300-300 and C300-500 (57%) and the minimum yield was 33% for all treatments (Fig. 2d).

This decrement in yield as the pyrolysis temperature increment, regardless of feedstock types and sizes, is logical due to the thermal decomposition of lignin and cellulose, loss of volatile matter and non-condensable gases with increasing the temperature. These results are in agreement with [6,8] who studied the yield of biochar produced from rapeseed stem in the temperature range (200–700 °C). They attributed this decrease to the loss of moisture and labile volatile matter. Moreover, Yu et al. [4] reported a decrease in the yield of biochar produced from hinoki cypress from 33% to 21% with increasing pyrolysis temperature from 350 to 600 °C, respectively as a result of decomposition progresses during the pyrolysis process. Similar results were obtained using Jift [43,44], date seeds [2] and

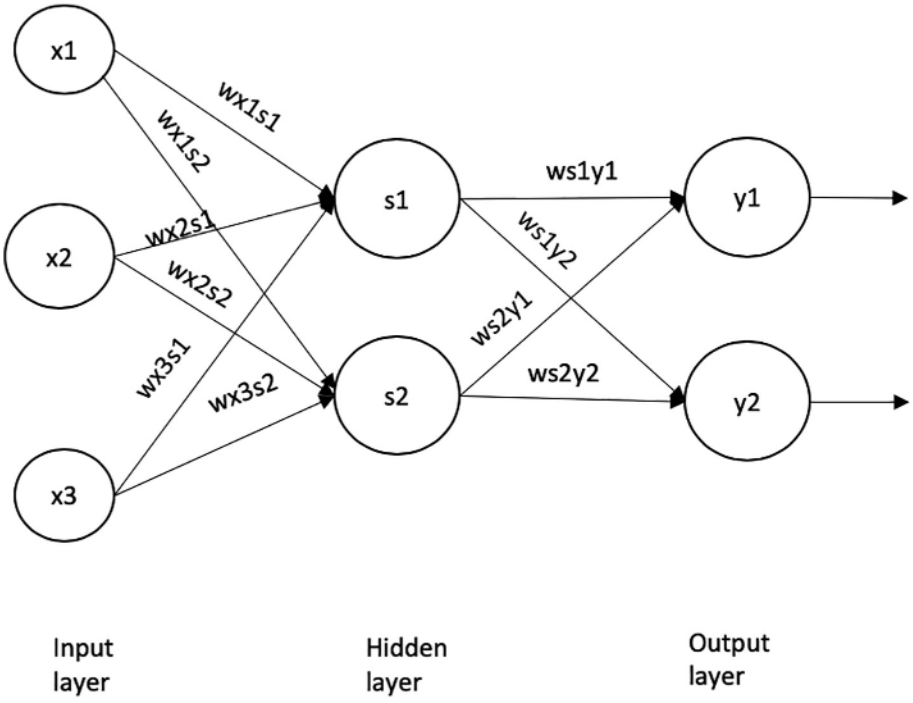

Fig. 1 General representation of an artificial neural network.

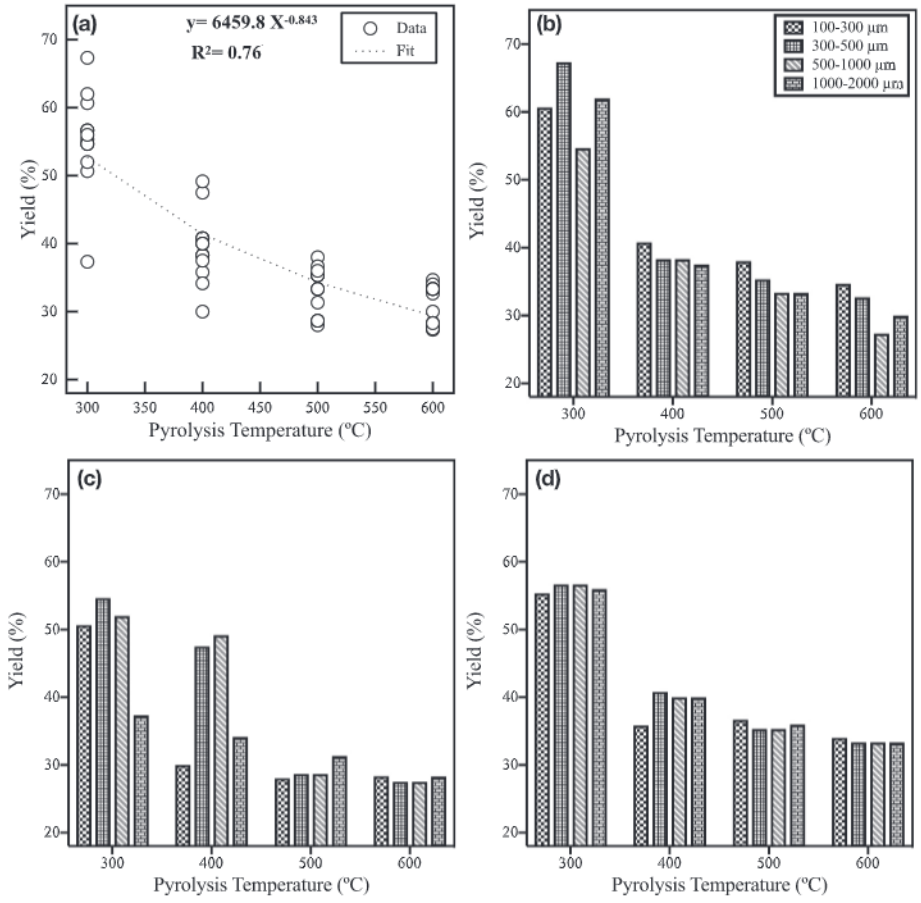

Fig. 2 Effect of pyrolysis temperature and feedstock size on biochar yield of (a) all treatments, (b) Oak acorns, (c) Jift and (d) Carob pods.

switchgrass, oak wood and biosolid [15]. Feedstock size affected the yield only marginally. The greatest effect was observed in the case of jift for the lower pyrolysis temperatures (300 and 400 °C). This may be due to the nature of the material separated in these sizes (100–300 and 1000–2000 μm). Jift is a complex inhomogeneous waste made up of olive skin, pomace and stone. Each component has different physical and chemical properties. Therefore, when subjected to grinding the different components may not reduce to the same size equally and may segregate when sieved. As a result, it is likely to obtain a sample with one component being overrepresented, thus resulting in greater variation in the yield, especially at lower pyrolysis temperatures. Nevertheless, this variation is minimized at higher temperatures due to abundance of energy to decompose the harder cellulosic materials.

3.2. Proximate analysis

Proximate analysis of biochar produced from Oak, Jift and Carob pods are tabulated in Tables 2–4 respectively. The results show that as pyrolysis temperature increased, the volatile matter content decreased while the fixed carbon content and hence the thermal stability of the biochar increased, regardless of feedstock type and size.

For instance, it was observed that when the pyrolysis temperature increased from 300 to 600 °C, the volatile matter content decreased from 50% to 11%, ash content increased from 8% to 25%, fixed carbon increased from 42% to 64% and thermal stability increased from 0.45 to 0.85 for the biochar produced from oak acorns of 100–300 μm size (Table 2).

Under same pyrolysis temperatures and feedstock size, the volatile matter content decreased from 71% to 46%, ash content increased from 9% to 14%, fixed carbon increased from 21% to 40% and thermal stability increased from 0.23 to 0.47 for the biochar produced from Jift of 100–300 μm size (Table 3).

Moreover, for the biochar produced from carob pods of 100–300 μm size, the volatile matter content decreased from 91% to 77%, ash content increased from 6% to 17%, fixed carbon increased from 3% to 6% and thermal stability increased from 0.03 to 0.07 (Table 4).

Table 2 Proximate analysis of biochar produced from Oak of different sizes at different pyrolysis temperatures.

Treatment	Ash (%)	VM (%)	FC (%)	TS
O300-100	8.03	50.44	41.5	0.45
O300-300	11.07	51.15	37.8	0.42
O300-500	8.08	55.12	36.8	0.40
O300-1000	13.06	45.70	41.2	0.47
O400-100	11.37	34.91	53.7	0.61
O400-300	11.76	34.85	47.5	0.58
O400-500	15.55	39.84	44.6	0.53
O400-1000	14.66	43.79	41.6	0.49
O500-100	20.62	22.06	57.3	0.72
O500-300	19.56	26.70	53.7	0.67
O500-500	19.65	32.14	48.2	0.60
O500-1000	24.48	36.16	39.4	0.52
O600-100	24.92	11.24	63.8	0.85
O600-300	21.42	10.61	68.0	0.87
O600-500	25.16	13.62	61.2	0.82
O600-1000	27.98	13.03	59.0	0.82

Table 3 Proximate analysis of biochar produced from Jift of different sizes at different pyrolysis temperatures.

Treatment	Ash (%)	VM (%)	FC (%)	TS
J300-100	8.67	70.60	20.7	0.23
J300-300	6.52	76.60	16.9	0.18
J300-500	7.16	72.40	20.4	0.22
J300-1000	5.54	50.70	43.8	0.46
J400-100	11.42	62.10	26.5	0.30
J400-300	7.72	66.90	25.4	0.28
J400-500	11.31	63.60	25.1	0.28
J400-1000	9.72	41.60	48.7	0.54
J500-100	12.97	54.10	32.9	0.38
J500-300	12.36	55.70	31.9	0.36
J500-500	12.97	50.00	37.0	0.43
J500-1000	11.79	38.20	50.0	0.57
J600-100	14.02	45.90	40.1	0.47
J600-300	13.88	46.30	39.8	0.46
J600-500	13.01	44.00	43.0	0.49
J600-1000	13.98	32.40	53.6	0.62

Table 4 Proximate analysis of biochar produced from Carob Pods of different sizes at different pyrolysis temperatures.

Treatment	Ash (%)	VM (%)	FC (%)	TS
C300-100	5.71	91.22	3.1	0.03
C300-300	6.35	90.34	3.3	0.04
C300-500	5.92	88.03	6.0	0.06
C300-1000	5.86	86.29	7.9	0.08
C400-100	9.34	82.21	8.5	0.09
C400-300	8.98	82.62	8.4	0.09
C400-500	9.12	79.96	10.9	0.12
C400-1000	9.06	79.31	11.6	0.13
C500-100	11.87	79.35	8.8	0.10
C500-300	10.09	76.35	13.6	0.15
C500-500	9.62	77.25	13.1	0.15
C500-1000	9.71	76.60	13.7	0.15
C600-100	16.99	76.92	6.1	0.07
C600-300	10.32	71.09	18.6	0.21
C600-500	11.69	70.69	17.6	0.20
C600-1000	12.59	70.87	16.5	0.19

Generally, volatile matter content, ash content, fixed carbon and thermal stability of the produced biochar ranged from 10–11%, 6–28%, 3–68% and 0.03–0.87, respectively, according to the pyrolysis temperature, feedstock types and sizes.

Given the same pyrolysis temperature, the ash content, VM, FC and TS of the biochar varied with feedstock size. For example, the FC showed a decreasing trend with feedstock size in case of oak, and for the case of the lower temperatures for carob. On the other hand, there seem to be no significant difference in the case of jift with the exception of the 1000–2 000 μm. This is probably due to the type of material retained in this particle size range, which is likely to be the harder component of the jift (olive seed and pomace).

The trend in the results mentioned above is in agreement with many researchers who concluded that increasing pyrolysis temperature led to a decrease in volatile matter content and increase in ash content and fixed carbon [4,8,25,45]. The decrement in volatile matter content that accompanies the increase in the pyrolysis temperature could be due to the destruction of

cellulose and hemicellulose moieties [46]. Ash content represents the inorganic fraction that cannot be volatilized or degraded by combustion and determines the biochar quality in a reverse relationship where the lower ash% the better the biochar quality [43]. Moreover, the high fixed carbon content and thermal stability after pyrolysis at higher pyrolysis temperature indicates a formation of thermally stable components that consists mainly of carbon [8], longer residence time in soil and more recalcitrant in the environment [3] demonstrating the role of biochar in C sequestration.

Of the three feedstock studied, oak acorn has the best potential for carbon sequestration in soil as it has the highest FC and TS (Table 2), followed by jift (Table 3) while carob is the least favorable (Table 4). Considering the ash content, carob-derived biochar has the lowest ash content making them the most suitable for agricultural applications.

3.3. Physiochemical characteristics of biochar

The effects of feedstock type, size and pyrolysis temperature on EC, pH, pH_{pzc} and SSA of biochar are presented in Tables 5–7. Electrical conductivity (EC), pH and SSA increased with increasing pyrolysis temperature for all combinations. The pH_{pzc} slightly decreased as the pyrolysis temperature increased. The particle size has marginal impact on the physiochemical characteristics of the biochar with its impact was most notable on the SSA, which decreased with the feedstock particle size.

Table 5 shows the effect of pyrolysis temperature and feedstock size on the EC, pH, pHpzc and SSA of the produced biochar from oak acorns. Generally, pH increased with increasing pyrolysis temperature for all biochar sizes. The highest pH value was 9.1 for biochar size 1000–2000 μm produced at 600 °C (O600-1000) whereas the lowest pH value was 5.7 for biochar size 1000–2000 μm produced at 300 °C (O300-1000). Moreover, there was no relationship between the pH and feedstock size. pH_{pzc} decreased with increasing pyrolysis temperature for all biochar sizes. The highest pH_{pzc} value was 8.9 for biochar size 1000–2000 μm produced at 300 °C (O300-1000) whereas the lowest pH_{pzc} value was 7.3 for biochar size 500–1000 μm produced at 600 °C (O600-500). Moreover, there was no relationship between the pH_{pzc} and feedstock size. SSA increased with increasing pyrolysis temperature for all biochar sizes. The highest SSA value was 194.5 m^2/g for biochar size 100–300 μm produced at 600 °C (O600-100) whereas the lowest SSA value was 134.7 m^2/g for biochar size 1000–2000 μm produced at 300 °C (O300-1000). Moreover, there was a decrease in SSA with increasing the biochar size at the same pyrolysis temperature. EC increased with increasing pyrolysis temperature for all biochar sizes. The highest EC value was 1652 μS/cm for biochar size 300–500 μm produced at 600 °C (O600-300) whereas the lowest EC value was 94 μS/cm for biochar size 1000–2000 μm produced at 300 °C (O300-1000). Moreover, there was no relationship between the EC and feedstock size. The EC correlates well with the ash content of the biochar.

Table 6 shows the effect of pyrolysis temperature and feedstock size on the pH, pH_{pzc}, SSA and EC of the produced bio-

Table 5 Effect of pyrolysis temperature and feedstock size on physiochemical characteristics of biochar produced from oak acorns.

Treatment	EC (μS/cm)	pH	pH_{pzc}	SSA (m^2/g)
O300-100	600	6.3	8.3	177.2
O300-300	373	6.0	8.7	175.4
O300-500	133	6.4	8.2	149.0
O300-1000	94	5.7	8.9	134.7
O400-100	1058	7.8	8.1	186.2
O400-300	572	8.5	8.4	182.3
O400-500	338	8.3	7.9	175.8
O400-1000	384	8.3	8.5	148.8
O500-100	1208	8.6	8.0	192.6
O500-300	637	8.5	8.4	189.8
O500-500	417	8.4	7.7	183.4
O500-1000	539	8.2	8.3	174.9
O600-100	1460	8.9	8.0	194.5
O600-300	1652	9.0	8.2	192.2
O600-500	1415	9.0	7.3	189.2
O600-1000	1474	9.1	8.1	179.8

Table 6 Effect of pyrolysis temperature and feedstock size on physiochemical characteristics of biochar produced from jift.

Treatment	EC (μS/cm)	pH	pH_{pzc}	SSA (m^2/g)
J300-100	959	8.3	9.5	166.6
J300-300	821	8.0	9.6	157.8
J300-500	637	8.6	9.7	143.8
J300-1000	261	7.4	9.0	112.7
J400-100	3620	9.2	8.7	171.6
J400-300	853	9.0	9.5	165.2
J400-500	691	8.6	9.3	160.9
J400-1000	1227	8.9	8.9	135.5
J500-100	4300	9.4	8.5	186.2
J500-300	3180	9.4	9.2	177.1
J500-500	3020	9.3	9.1	171.8
J500-1000	2019	8.9	8.5	168.5
J600-100	5700	9.4	8.0	187.3
J600-300	5630	9.7	8.4	186.8
J600-500	4460	9.5	8.6	176.9
J600-1000	3110	9.3	8.5	173.6

Table 7 Effect of pyrolysis temperature and feedstock size on physiochemical characteristics of biochar produced from jift.

Treatment	EC (μS/cm)	pH	pH_{pzc}	SSA (m^2/g)
C300-100	1481	6.9	8.5	162.3
C300-300	1620	6.6	8.6	157.2
C300-500	1414	6.8	8.5	151.0
C300-1000	1001	6.8	11.3	144.0
C400-100	2410	8.5	8.4	173.3
C400-300	2420	9.0	8.6	165.6
C400-500	3970	8.8	8.1	155.4
C400-1000	2570	9.0	10.1	152.3
C500-100	3470	9.2	8.1	181.5
C500-300	3770	9.0	8.2	173.8
C500-500	4130	9.3	8.0	157.9
C500-1000	3480	9.1	9.8	157.3
C600-100	5580	9.3	7.9	191.5
C600-300	4680	9.5	8.0	180.4
C600-500	5250	9.3	7.8	176.3
C600-1000	4760	9.6	9.6	168.5

char from jift. Generally, pH increased with increasing pyrolysis temperature for all biochar sizes. The highest pH value was 9.7 for biochar size 300–500 μm produced at 600 °C (J600-300) whereas the lowest pH value was 7.4 for biochar size 1000–2000 μm produced at 300 °C (J300-1000). Moreover, there was no relationship between the pH and feedstock size. pH_{pzc} decreased with increasing pyrolysis temperature for all biochar sizes. The highest pH_{pzc} value was 9.7 for biochar size 500–1000 μm produced at 300 °C (J300-500) whereas the lowest pH_{pzc} value was 8 for biochar size 100–300 μm produced at 600 °C (J600-100). Moreover, there was no relationship between the pH_{pzc} and feedstock size. SSA increased with increasing pyrolysis temperature for all biochar sizes. The highest SSA value was 187.3 m^2/g for biochar size 100–300 μm produced at 600 °C (J600-100) whereas the lowest SSA value was 112.7 m^2/g for biochar size 1000–2000 μm produced at 300 °C (J300-1000). Moreover, there was a decrease in SSA with increasing the biochar size at the same pyrolysis temperature. EC increased with increasing pyrolysis temperature for all biochar sizes. The highest EC value was 5700 μS/cm for biochar size 100–300 μm produced at 600 °C (J600-100) whereas the lowest EC value was 261 μS/cm for biochar size 1000–2000 μm produced at 300 °C (J300-1000). The table shows an inverse relation between feedstock size and EC, nevertheless, feedstock size is a surrogate parameter and the actual relationship is between the EC and the ash content rather than feedstock size.

Table 7 shows the effect of pyrolysis temperature and feedstock size on the pH, pH_{pzc}, SSA and EC of the produced biochar from carob pods. Generally, pH increased with increasing pyrolysis temperature for all biochar sizes. The highest pH value was 9.6 for biochar size 1000–2000 μm produced at 600 °C (C600-1000) whereas the lowest pH value was 6.6 for biochar size 300–500 μm produced at 300 °C (C300-300). Moreover, there was no relationship between the pH and feedstock size. pH_{pzc} decreased with increasing pyrolysis temperature for all biochar sizes. The highest pH_{pzc} value was 11.3 for biochar size 1000–2000 μm produced at 300 °C (C300-1000) whereas the lowest pH_{pzc} value was 7.8 for biochar size 500–1000 μm produced at 600 °C (C600-500). Moreover, there was no relationship between the pH_{pzc} and feedstock size. SSA increased with increasing pyrolysis temperature for all biochar sizes. The highest SSA value was 191.5 m^2/g for biochar size 100–300 μm produced at 600 °C (C600-100) whereas the lowest SSA value was 144.0 m^2/g for biochar size 1000–2000 μm produced at 300 °C (C300-1000). Moreover, there was a decrease in SSA with increasing the biochar size at the same pyrolysis temperature. EC increased with increasing pyrolysis temperature for all biochar sizes. The highest EC value was 5580 μS/cm for biochar size 100–300 μm produced at 600 °C (C600-100) whereas the lowest EC value was 1001 μS/cm for biochar size 1000–2000 μm produced at 300 °C (C300-1000).

The pH results of this study came in line with the published results in the literature where a positive correlation between pH and pyrolysis temperature exists. The pH values of the biochar tend to be high and alkaline. The positive correlation between alkalinity and pyrolysis temperature is explained by three reasons: (1) the alkali salts exists in the ash, which increase pyrolysis temperature increases (Tables 2–4); (2) the high densities of acidic functional groups on the surface of the produced biochar at lower pyrolysis temperatures and (3) the increase of inorganic carbonates with increasing pyrolysis temperatures [6,21,45–47].

There is a crucial role for pH_{pzc} in selecting the optimal pH value for adsorption studies and explaining the mechanisms of adsorption [45]. The pH_{pzc} values were approximately 8.2, 8.9 and 8.7 for biochar produced from oak acorns, jift and carob pods, respectively. Therefore, pH values of a solution should be maintained above the value of pH_{pzc} ($pH_{solution} > pH_{pzc}$) to ensure a negatively charged surface of biochar which makes it favorable to adsorb cations such as heavy metals and cationic dyes due to the ionization or dissociation of acidic oxygen surface groups. When $pH_{solution} < pH_{pzc}$, the biochar surface is a positively charged due to the protonation of the acidic groups which makes it favorable to adsorb anions such as PO_4^{-3} [45,48].

Overall, it was observed that the SSA was positively correlated with the pyrolysis temperature and negatively correlated with particle size. For example, the SSA of the biochar produced from oak acorn at 300 °C and particle size 100–300 μm is 177.2 m^2/g which is 91% of that produced from the same biomass but at 600 °C. With regard to particle size, the SSA of the same biochar is around 132% of that produced from the same biomass but larger particle size (1000–2000 μm). However, the gap between the SSA of the smaller size biomass derived biochar and that produced from larger particle sizes, narrows as the pyrolysis temperature increases.

ANOVA analysis suggested that the effect of particle size and pyrolysis temperature on the characteristics of the biochar varied according to the treated biomass. For example, in the case of oak acorn and carob pods derived biochar, particle size had a significant ($a < 0.05$) effect on the pH_{pzc} while pyrolysis temperature affected the SSA. On the other hand, there were no significant differences observed in the pH_{pzc} and SSA among biochar produced from different particle sizes but differences were observed among biochar produced at different pyrolysis temperatures.

Specific surface area results of this study confirmed the literature results of the positive correlation between specific surface area and pyrolysis temperature [2,3,6,8,44]. For example, SSA range from 16.2 to 397.4 m^2/g for the biochar produced at 350 and 750 °C, respectively [3]. Similarly, SSA increased from 11.9 to 545.4 m^2/g after increasing pyrolysis temperature from 400 to 800 °C [29]. This increase in SSA could be explained by pores creation through the volatilization of compounds as illustrated in Tables 2–4 [6,49].

The increment in the EC values with increasing pyrolysis temperatures is well documented in the literature [3,23,25,43,44,50]. For example, EC value increased from 1280, 2710, 2990 to 4390 μS/cm after increasing the pyrolysis temperature from 350, 350, 550 to 630 °C, respectively [44]. This increase is the result of increasing salts existing in the ash fraction, which increase with increasing the pyrolysis temperature (Table 2–4) [23,45,46]. Variations of the electrical conductivity between the different feedstocks could be explained by the nutrient content of each feedstock.

3.4. FTIR analysis

The FTIR analysis of biochar produced from the different feedstocks at 300 and 600 °C of 100–300 and 1000–2000 μm are presented in Table 8. FTIR analysis was carried out to

Table 8 FTIR peaks observed for selected biochar samples.

	C300-1000	C300-100	C600-1000	C600-100	J300-1000	J300-100	J600-1000	J600-100	O300-1000	O300-100	O600-1000	O600-100
Alkanes	X	X	X	X	X	X	X	X	X	X	X	X
Alkenes	X	X	X	X		X	X	X			X	X
Alkynes											X	
Arenes	X	X		X		X	X	X		X	X	
Alcohol & Phenols	X	X			X	X			X	X		
Amines					X	X					X	
Aldehydes & Ketones	X	X	X	X	X	X			X	X		
Carbonyl	X	X			X	X	X		X	X	X	X

characterize the surface organic functional groups present on the produced biochar. All chars were rich with surface functional groups including hydroxyl and carbonyl groups, which can provide active adsorption sites. Hydroxyl groups were easily identifiable in all chars prepared at 300 °C but absent from those prepared at 600 °C, which is likely due to better carbonization.

Although some minor variations in the type of functional groups present, the particle size seems to have very little effect. Nevertheless, some notable variations can be observed between O600-1000 and O600-100. The O600-1000 displayed a wider variety of surface functional groups than the O600-100, this could be due to heat transfer variation which may have led to variation in the carbonization degree along the diameter of the oak particle. The layers closer to the surface were more exposed to the heat and therefore had better carbonization, this layer could form a natural insulation which could affect the diffusion of the heat to the inner surfaces and in turn those would experience lower carbonization degree. Subsequently, different functional groups could form depending on the carbonization degree. This is also observed, although to a lesser degree, in the case of the Carob prepared at 600 °C and the Jift. Pyrolysis temperature has a prominent effect on the surface functional groups with pronounced differences between chars prepared at 300 °C and those prepared at 600 °C. The most notable difference is the disappearance of the band corresponding to the hydroxyl group from all chars prepared at 600 °C. Also, variations are observed in the carbonyl functional groups with bands corresponding to esters, ketones and aldehydes disappearing from the oak and jift chars prepared at 600 °C.

3.5. Artificial neural network modeling

In this study, the aim of the model was to predict the adsorption capacity of biochar given its parent biomass type, particle size, the pyrolysis temperature it was prepared at and the initial concentration of adsorbate. For this purpose, Matlab™ nftool was used to build the model. However, two input variables (biomass type and particle size range) were not of rational data type. Matlab™ nftool only accepts numerical values, therefore it was necessary to convert these values into a data type acceptable by the tool. The biomass type is categorical data and it would not make sense to convert it to a number (say integer) as this may introduce bias due to magnitude. Thus, a coding system that will not introduce bias into the model was adopted. Each biomass type was represented by a 1×3 vector of zeros and ones as follows: Carob = [0 0 1]; Jift = [0 1 0] and Oak = [1 0 0]. The particle size data, on the other hand, may be seen as ordinal; however, due to the significant differences in the ranges, using the mean or other concentric value may not be representative and may introduce bias, so they too were represented as 1×4 vectors of zeros and ones. The 100–300 range was represented as [0 0 0 1], the 300–500 range as [0 0 1 0], the 500–1000 range as [0 1 0 0] and the 1000–2000 range as [1 0 0 0]. At the end, the input matrix had 9 columns representing the four independent variables.

The target values were collected by conducting batch adsorption studies for each biochar using methylene blue concentrations ranging from 1 to 5 mM at neutral pH ~ 6.5 as described earlier. In total, 720 data sets were collected representing (3 biomass types × 4 particle sizes × 4 pyrolysis temperatures × 5 concentrations × 3 triplicates for each biochar). So, the input matrix size was 720×9 and the target matrix contained the corresponding qe values, a vector of 720×1. The data was randomly divided into 3 sets; 70% for training the network, 15% for validation and 15% for testing.

To optimize the performance of the network, the number of neurons in the hidden layer must be determined. It is important to keep the number of neurons to the minimum to avoid overtraining. In our case we tested 1, 3, 5 and 7 neurons. The performance of the network was measured using the coefficient of correlation (R) and the mean squared error (MSE), coefficient of determination (R^2) and root mean squared error (RMSE).

$$R = \frac{n\sum xy - \sum x \sum y}{\sqrt{(n\sum x^2 - \sum x^2)(n\sum y^2 - (\sum y)^2)}}$$

$$MSE = \frac{1}{n}\sum (x_p - x_o)^2$$

$$RMSE = \sqrt{MSE}$$

where $\bar{x}, \bar{y}$ are the average values of x and y, respectively; x_p and x_o are the predicted and observed value, respectively; n is the number of observations.

The network was trained using the Levenberg-Marquardt back propagation algorithm (Fig. 3). The Transfer functions

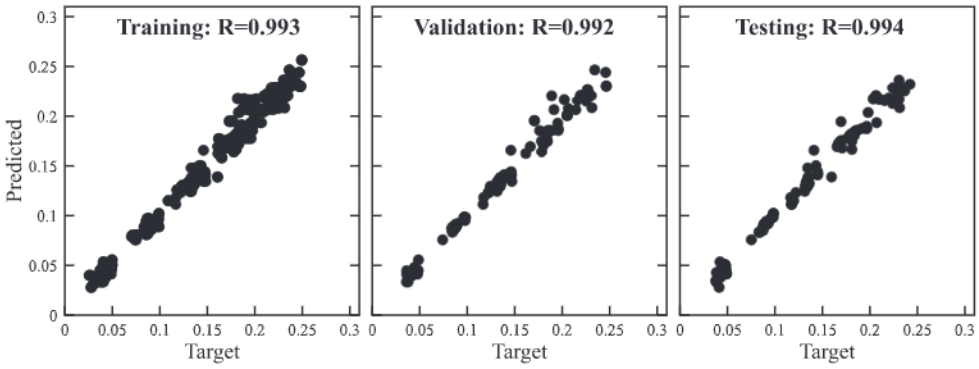

Fig. 3 Model training, validation and test results.

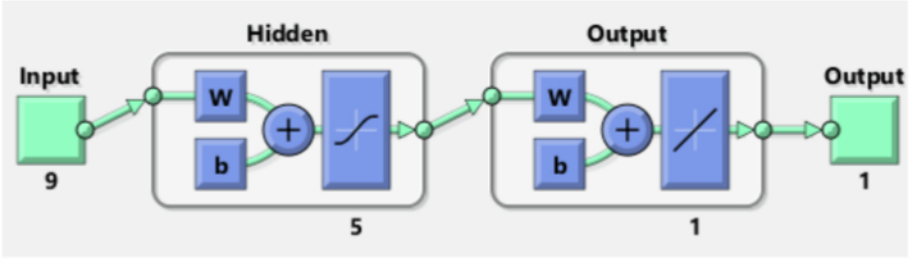

Fig. 4 Matlab™ representation of the neural network model.

used were the Sigmoid Symmetric (tansig) for the hidden layer and purelin for the output layer. The best performance for the training was achieved with 5 neurons in the hidden ($R = 0.9937$ and $MSE = 5.27 \times 10^{-5}$) which means that the model is able to explain 98.7% of the variability of the adsorption capacity ($R^2 = 0.987$) with high precision ($RMSE = 0.007$ mmol/g). The Matlab™ typology of the model is shown in Fig. 4.

The developed model was successful in predicting the adsorption capacity of the biochar, as shown in Fig. 5. The output of the model strongly correlates to the observed values ($R = 0.993$, $MSE = 5.34 \times 10^{-5}$).

To see how the model will predict specific sets, it was tested on selected biochars. For example, the Fig. 6 shows how well does the model predict the adsorption capacity of biochars prepared from the Carob parent biomass at 300 °C of particle size in the range 100–300 µm and MB concentrations between 1 and 5 mM ($R = 0.974$, $MSE = 2.41 \times 10^{-4}$). The model was also tested for its predictability of the biochar derived from Jift, with particle size between 300 and 500 µm, prepared at pyrolysis temperature 400 °C and MB concentration 1 mmol. The average adsorption capacity obtained from the experiments was 0.0473 $mmol.g^{-1}$ with standard deviation 9.1×10^{-4}. The model slightly underestimated the capacity

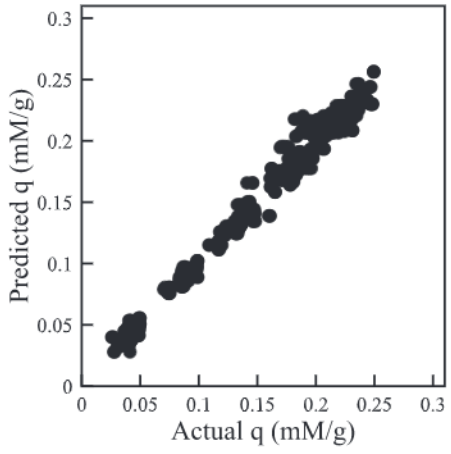

Fig. 5 Model performance using the entire set.

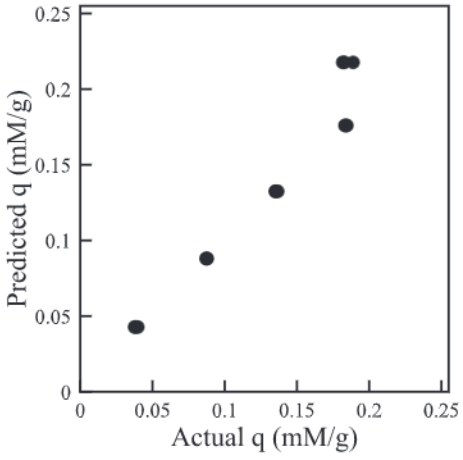

Fig. 6 Models prediction for adsorption capacity of Carob derived biochar with particle size range 100–300 µm, pyrolysis temperature 300 °C and MB concentrations between 1 and 5 mM.

at 0.045 mmol.g^{-1} which represents an absolute relative error < 5%.

To further demonstrate the usefulness of the model, it was used to estimate the adsorption capacity of oak-derived biochar with particle size 500–1000 μm prepared at 450 °C and MB concentration 5 mM. The model predicted the adsorption capacity to be 0.227 mmol.g^{-1}. This is a very reasonable prediction, given that the observed mean adsorption capacities for this biochar at 400 and 500 °C are 0.225 and 0.227 mmol.g^{-1}, respectively. The model can also be used to predict the adsorption capacities of any combinations of biomass, particles sizes and MB concentrations. For example, the model predicts that a biochar with particle size range 300–1000 mm, prepared at 650 °C and derived from oak acorn and carob will have adsorption capacity of 0.388 mmol.g^{-1} when used to treat water contaminated with MB with a concentration = 3.1 mmol.L^{-1}. Hence, the model may be used to design specific biochars and predict their performance before actual synthesis.

4. Conclusions

The properties of biochar produced from different feedstocks types and sizes under slow pyrolysis conditions of different temperatures were investigated. Pyrolysis temperature affected the biochar characteristics. The activity of the biochar was tested by its methylene blue adsorption capacity. Methylene blue adsorption is a good indicator of the biochar quality. An artificial neural network model was developed to predict the methylene blue adsorption capacity of the biochar based on the parent biomass type and particle size, pyrolysis temperature and initial methylene blue concentration. The model is useful to forecast the quality of biochar and design the biochar to meet the specific targeted concentration of the pollutant. It can reduce the laborious work of biochar production and adsorption experiments. However, the model is limited by the types of biomass. Nevertheless, the model can be easily retrained to accommodate new biomass types. It is suggested that more biomass types are added in the future. It is further suggested to extend the model to include other pollutants.

Funding

This research was funded by Deanship of Research at Jordan University of Science and Technology (JUST), grant number 336/2015.

CRediT authorship contribution statement

Ammar Albalasmeh: Conceptualization, Methodology, Supervision, Writing - original draft, Writing - review & editing, Project administration, Funding acquisition, Formal analysis, Visualization, Resources. **Mamoun A. Gharaibeh:** Methodology, Writing - review & editing. **Osama Mohawesh:** Formal analysis, Writing - review & editing. **Mohammad Ajlouni:** Investigation, Visualization. **Mohammed Quzaih:** Investigation, Visualization. **Mohanad Masad:** Writing - review & editing. **Ali El Hanandeh:** Conceptualization, Methodology, Writing - original draft, Writing - review & editing, Formal analysis, Data curation, Software.

Acknowledgments

The authors would like to acknowledge the Deanship of Research at JUST for the financial support of this study. The authors would also like to thank Miss Balqis El Hanandeh for proofreading the manuscript.

Conflicts of interest

The authors declare no conflict of interest.

References

[1] J. Schellekens, C.A. Silva, P. Buurman, T.F. Rittl, R.R. Domingues, M. Justi, P. Vidal-Torrado, P.F. Trugilho, Molecular characterization of biochar from five Brazilian agricultural residues obtained at different charring temperatures, J. Anal. Appl. Pyrolysis 130 (2018) 249–255, https://doi.org/10.1016/j.jaap.2018.01.020.

[2] Z. Mahdi, A. El Hanandeh, Q. Yu, Influence of pyrolysis conditions on surface characteristics and methylene blue adsorption of biochar derivedfrom date seed biomass, waste and biomass, Valorization (2016) 1–13.

[3] M. Askeland, B. Clarke, J. Paz-Ferreiro, Comparative characterization of biochars produced at three selected pyrolysis temperatures from common woody and herbaceous waste streams, PeerJ 7 (2019) 1–20, https://doi.org/10.7717/peerj.6784.

[4] S. Yu, J. Park, M. Kim, C. Ryu, J. Park, Characterization of biochar and byproducts from slow pyrolysis of hinoki cypress, Bioresour. Technol. Rep. 6 (2019) 217–222, https://doi.org/10.1016/j.biteb.2019.03.009.

[5] C. Zavalloni, G. Alberti, S. Biasiol, G.D. Vedove, F. Fornasier, J. Liu, A. Peressotti, Microbial mineralization of biochar and wheat straw mixture in soil: a short-term study, Appl. Soil Ecol. 50 (2011) 45–51, https://doi.org/10.1016/J.APSOIL.2011.07.012.

[6] B. Zhao, D. O'Connor, J. Zhang, T. Peng, Z. Shen, D.C.W. Tsang, D. Hou, Effect of pyrolysis temperature, heating rate, and residence time on rapeseed stem derived biochar, J. Clean. Prod. 174 (2018) 977–987, https://doi.org/10.1016/j.jclepro.2017.11.013.

[7] J. Lehmann, S. Joseph, Biochar for environmental management: science and technology, (2009).

[8] X. Yang, W. Ng, B.S.E. Wong, G.H. Baeg, C.H. Wang, Y.S. Ok, Characterization and ecotoxicological investigation of biochar produced via slow pyrolysis: effect of feedstock composition and pyrolysis conditions, J. Hazard. Mater. 365 (2019) 178–185, https://doi.org/10.1016/j.jhazmat.2018.10.047.

[9] A. El Hanandeh, A.A. Albalasmeh, M. Gharaibeh, Phosphorus removal from wastewater in biofilters with biochar augmented geomedium: effect of biochar particle size, Clean - Soil Air Water (2017), https://doi.org/10.1002/clen.201600123.

[10] A. El Hanandeh, M. Gharaibeh, A.A. Albalasmeh, Phosphorus removal efficiency from wastewater under different loading conditions using sand biofilters augmented with biochar, Int. J. Environ. Sci. Technol. 15 (2018), https://doi.org/10.1007/s13762-017-1474-0.

[11] D.V. Sarkhot, A.A. Berhe, T.A. Ghezzehei, Impact of biochar enriched with dairy manure effluent on carbon and nitrogen dynamics, J. Environ. Qual. 41 (2012) 1107.

[12] D.V. Sarkhot, T.A. Ghezzehei, A.A. Berhe, Effectiveness of biochar for sorption of ammonium and phosphate from dairy effluent, J. Environ. Qual. 42 (2013) 1545.

[13] G. Agegnehu, A.M. Bass, P.N. Nelson, B. Muirhead, G. Wright, M.I. Bird, Biochar and biochar-compost as soil amendments:

effects on peanut yield, soil properties and greenhouse gas emissions in tropical North Queensland, Australia, Agric. Ecosyst. Environ. 213 (2015) 72–85, https://doi.org/10.1016/J.AGEE.2015.07.027.
[14] K.C. Uzoma, M. Inoue, H. Andry, A. Zahoor, E. Nishihara, Influence of biochar application on sandy soil hydraulic properties and nutrient retention, J. Food Agric. Environ. 9 (2011) 1137–1143.
[15] S. Li, G. Chen, Thermogravimetric, thermochemical, and infrared spectral characterization of feedstocks and biochar derived at different pyrolysis temperatures, Waste Manag. 78 (2018) 198–207, https://doi.org/10.1016/j.wasman.2018.05.048.
[16] J.M. Novak, I.M. Lima, B. Xing, J. Gaskin, C. Steiner, K.C. Das, M. Ahmedna, D. Rehrah, D.W. Watts, W.J. Busscher, H. Schomberg, Characterization of designer biochar produced at different temperatures, Ann. Environ. Sci. 3 (2009) 195–206.
[17] M. Ahmad, A.U. Rajapaksha, J.E. Lim, M. Zhang, N. Bolan, D. Mohan, M. Vithanage, S.S. Lee, Y.S. Ok, Biochar as a sorbent for contaminant management in soil and water: a review, Chemosphere 99 (2014) 19–33, https://doi.org/10.1016/J.CHEMOSPHERE.2013.10.071.
[18] G. Gascó, J. Paz-Ferreiro, M.L. Álvarez, A. Saa, A. Méndez, Biochars and hydrochars prepared by pyrolysis and hydrothermal carbonisation of pig manure, Waste Manag. 79 (2018) 395–403, https://doi.org/10.1016/J.WASMAN.2018.08.015.
[19] H.P. Lu, Z.A. Li, G. Gascó, A. Méndez, Y. Shen, J. Paz-Ferreiro, Use of magnetic biochars for the immobilization of heavy metals in a multi-contaminated soil, Sci. Total Environ. 622–623 (2018) 892–899, https://doi.org/10.1016/J.SCITOTENV.2017.12.056.
[20] A.E. Hanandeh, R.A. Abu-Zuryk, I. Hamdneh, A.H. Al-Dujaili, Characterization of biochar prepared from slow pyrolysis of Jordanian olive oil processing solid waste and adsorption efficiency of Hg2+ ions in aqueous solutions, Water Sci. Technol. (2016).
[21] J.-H. Yuan, R.-K. Xu, H. Zhang, The forms of alkalis in the biochar produced from crop residues at different temperatures, Bioresour. Technol. 102 (2011) 3488–3497, https://doi.org/10.1016/J.BIORTECH.2010.11.018.
[22] E.F. Zama, Y.-G. Zhu, B.J. Reid, G.-X. Sun, The role of biochar properties in influencing the sorption and desorption of Pb(II), Cd(II) and As(III) in aqueous solution, J. Clean. Prod. 148 (2017) 127–136, https://doi.org/10.1016/J.JCLEPRO.2017.01.125.
[23] J.A. Alburquerque, M.E. Sánchez, M. Mora, V. Barrón, Slow pyrolysis of relevant biomasses in the Mediterranean basin. Part 2. Char characterisation for carbon sequestration and agricultural uses, J. Clean. Prod. 120 (2016) 191–197, https://doi.org/10.1016/j.jclepro.2014.10.080.
[24] T.A. Ghezzehei, D.V. Sarkhot, A.A. Berhe, Biochar can be used to capture essential nutrients from dairy wastewater and improve soil physico-chemical properties, Solid Earth 5 (2014) 953–962.
[25] K. Intani, S. Latif, Z. Cao, J. Müller, Characterisation of biochar from maize residues produced in a self-purging pyrolysis reactor, Bioresour. Technol. 265 (2018) 224–235, https://doi.org/10.1016/j.biortech.2018.05.103.
[26] Y. Jin, X. Liang, M. He, Y. Liu, G. Tian, J. Shi, Manure biochar influence upon soil properties, phosphorus distribution and phosphatase activities: a microcosm incubation study, Chemosphere 142 (2016) 128–135, https://doi.org/10.1016/J.CHEMOSPHERE.2015.07.015.
[27] K.Y. Chan, L. Van Zwieten, I. Meszaros, A. Downie, S. Joseph, Using poultry litter biochars as soil amendments, Aust. J. Soil Res. 46 (2008) 437.
[28] S. Gul, J.K. Whalen, B.W. Thomas, V. Sachdeva, H. Deng, Physico-chemical properties and microbial responses in biochar-amended soils: mechanisms and future directions, Agric. Ecosyst. Environ. 206 (2015) 46–59, https://doi.org/10.1016/J.AGEE.2015.03.015.
[29] K. Jindo, H. Mizumoto, Y. Sawada, M.A. Sanchez-Monedero, T. Sonoki, Physical and chemical characterization of biochars derived from different agricultural residues, Biogeosciences 11 (2014) 6613–6621.
[30] F. Raposo, M.A. De La Rubia, R. Borja, Methylene blue number as useful indicator to evaluate the adsorptive capacity of granular activated carbon in batch mode: Influence of adsorbate/adsorbent mass ratio and particle size, J. Hazard. Mater. 165 (2009) 291–299, https://doi.org/10.1016/J.JHAZMAT.2008.09.106.
[31] M.A. Islam, M.J. Ahmed, W.A. Khanday, M. Asif, B.H. Hameed, Mesoporous activated coconut shell-derived hydrochar prepared via hydrothermal carbonization-NaOH activation for methylene blue adsorption, J. Environ. Manage. 203 (2017) 237–244, https://doi.org/10.1016/J.JENVMAN.2017.07.029.
[32] Y. Wang, R. Liu, Comparison of characteristics of twenty-one types of biochar and their ability to remove multi-heavy metals and methylene blue in solution, Fuel Process. Technol. 160 (2017) 55–63, https://doi.org/10.1016/J.FUPROC.2017.02.019.
[33] A.M. Ghaedi, A. Vafaei, Applications of artificial neural networks for adsorption removal of dyes from aqueous solution: a review, Adv. Colloid Interface Sci. 245 (2017) 20–39, https://doi.org/10.1016/J.CIS.2017.04.015.
[34] H. Karimi, M. Ghaedi, Application of artificial neural network and genetic algorithm to modeling and optimization of removal of methylene blue using activated carbon, J. Ind. Eng. Chem. 20 (2014) 2471–2476, https://doi.org/10.1016/J.JIEC.2013.10.028.
[35] N. Mahmoodi-Babolan, A. Heydari, A. Nematollahzadeh, Removal of methylene blue via bioinspired catecholamine/starch superadsorbent and the efficiency prediction by response surface methodology and artificial neural network-particle swarm optimization, Bioresour. Technol. 294 (2019), https://doi.org/10.1016/J.BIORTECH.2019.122084 122084.
[36] L.Y. Jun, R.R. Karri, L.S. Yon, N.M. Mubarak, C.H. Bing, K. Mohammad, P. Jagadish, E.C. Abdullah, Modeling and optimization by particle swarm embedded neural network for adsorption of methylene blue by jicama peroxidase immobilized on buckypaper/polyvinyl alcohol membrane, Environ. Res. 183 (2020), https://doi.org/10.1016/J.ENVRES.2020.109158 109158.
[37] P.R. Souza, G.L. Dotto, N.P.G. Salau, Artificial neural network (ANN) and adaptive neuro-fuzzy interference system (ANFIS) modelling for nickel adsorption onto agro-wastes and commercial activated carbon, J. Environ. Chem. Eng. 6 (2018) 7152–7160, https://doi.org/10.1016/J.JECE.2018.11.013.
[38] S. Rajkovich, A. Enders, K. Hanley, C. Hyland, A.R. Zimmerman, J. Lehmann, Corn growth and nitrogen nutrition after additions of biochars with varying properties to a temperate soil, Biol. Fertil. Soils 48 (2012) 271–284, https://doi.org/10.1007/s00374-011-0624-7.
[39] N. Fiol, V. Isabel, Determination of sorbent point zero charge: usefulness in sorption studies, Environ. Chem. Lett. 7 (2008) 79–84.
[40] A. Méndez, J. Paz-Ferreiro, F. Araujo, G. Gascó, Biochar from pyrolysis of deinking paper sludge and its use in the treatment of a nickel polluted soil, J. Anal. Appl. Pyrolysis 107 (2014) 46–52, https://doi.org/10.1016/j.jaap.2014.02.001.
[41] C.A. Nunes, M.C. Guerreiro, Estimation of surface area and pore volume of activated carbons by methylene blue and iodine numbers, Quimica (2011).
[42] J. Moreno-Pérez, A. Bonilla-Petriciolet, D.I. Mendoza-Castillo, H.E. Reynel-Ávila, Y. Verde-Gómez, R. Trejo-Valencia, Artificial neural network-based surrogate modeling of multi-component dynamic adsorption of heavy metals with a biochar,

J. Environ. Chem. Eng. 6 (2018) 5389–5400, https://doi.org/10.1016/J.JECE.2018.08.038.

[43] A. Hmid, D. Mondelli, S. Fiore, F.P. Fanizzi, Z. Al Chami, S. Dumontet, Production and characterization of biochar from three-phase olive mill waste through slow pyrolysis, Biomass (2014) 330–339.

[44] A. El Hanandeh, R. Abu-Zurayk, I. Hamadneh, A. Al-Dujaili, Characterization of biochar prepared from slow pyrolysis of Jordanian olive oil processing solid waste and adsorption efficiency of Hg2+ ions in aqueous solutions, Water Sci. Technol. 74 (2016) 1899–1910, https://doi.org/10.2166/wst.2016.378.

[45] H.N. Tran, S.-J. You, H.-P. Chao, Effect of pyrolysis temperatures and times on the adsorption of cadmium onto orange peel derived biochar, Waste Manag. Res. 34 (2016) 129–138, https://doi.org/10.1177/0734242X15615698.

[46] W.-K. Kim, T. Shim, Y.-S. Kim, S. Hyun, C. Ryu, Y.-K. Park, J. Jung, Characterization of cadmium removal from aqueous solution by biochar produced from a giant Miscanthus at different pyrolytic temperatures, Bioresour. Technol. 138 (2013) 266–270, https://doi.org/10.1016/j.biortech.2013.03.186.

[47] M. Keiluweit, P.S. Nico, M.G. Johnson, M. Kleber, Dynamic molecular structure of plant biomass-derived black carbon (biochar), Environ. Sci. Technol. 44 (2010) 1247–1253.

[48] Y. Liu, X. Zhao, J. Li, D. Ma, R. Han, Characterization of bio-char from pyrolysis of wheat straw and its evaluation on methylene blue adsorption, Desalin. Water Treat. 46 (2012) 115–123, https://doi.org/10.1080/19443994.2012.677408.

[49] U. Kumar, S. Maroufi, R. Rajarao, M. Mayyas, I. Mansuri, R. K. Joshi, V. Sahajwalla, Cleaner production of iron by using waste macadamia biomass as a carbon resource, J. Clean. Prod. 158 (2017) 218–224, https://doi.org/10.1016/j.jclepro.2017.04.115.

[50] A.R.A. Usman, A. Abduljabbar, M. Vithanage, Y.S. Ok, M. Ahmad, M. Ahmad, J. Elfaki, S.S. Abdulazeem, M.I. Al-Wabel, Biochar production from date palm waste: charring temperature induced changes in composition and surface chemistry, J. Anal. Appl. Pyrolysis 115 (2015) 392–400.